Structural properties and multiferroic phase diagram of $K_{0.6}Fe^{II}_{0.6}Fe^{III}_{0.4}F_3$ fluoride with TTB structure

F. Mezzadri,[1] S. Fabbrici,[1] E. Montanari,[1] L. Righi,[1] G. Calestani,[1,2,*] E. Gilioli,[2] F. Bolzoni,[2] and A. Migliori[3]
[1]*Dipartimento di Chimica GIAF, Università di Parma, Viale G.P. Usberti 17A, I-43100 Parma, Italy*
[2]*CNR-IMEM, Parco Area delle Scienze 37/A, I-43100 Parma, Italy*
[3]*CNR-IMM, Via Gobetti 101, I-40126 Bologna, Italy*
(Received 6 May 2008; published 15 August 2008)

Iron fluorides with tetragonal tungsten bronze (TTB) structure, having general formula of $K_xFe^{II}_xFe^{III}_{1-x}F_3$ with $0.4<x<0.6$, are possible candidates for complete multiferroism (elastic, electric, and magnetic orders) coupled with charge ordering phenomena. Following the indication of a previous general work, we concentrated our attention on the potassium rich region of these bronzes where an orthorhombic distortion of the fundamental TTB structure takes place. We tried to define the complex phase diagram of $K_{0.6}FeF_3$, involving the different ordering phenomena in the range of 5–600 K, by using a series of characterization techniques such as transmission electron microscopy, x-ray and neutron diffractions, and magnetic measurements. The results revealed the coexistence of all these orders below the magnetic transition occurring at 118 K, showing the unique behavior of a system that can be considered a model for multiferroism.

DOI: 10.1103/PhysRevB.78.064111 PACS number(s): 61.05.cp, 61.05.fm, 61.05.jm

I. INTRODUCTION

The term "tetragonal tungsten bronze" (TTB), originally utilized to indicate the nonstoichiometric compound $K_xWO_3(x=0.4-0.6)$, is usually extended to all the compounds showing a similar structure. By substituting tungsten with other high valence transition metals and potassium with Li, Na, Ba, Sr, and Pb ions, the TTB family includes today a large number of functional crystals and materials possessing electro-optic, ferroelectric (FE), ferroelastic (FEL), pyroelectric, and piezoelectric properties. For example, the ferroelectric-ferroelastic niobates crystallizing in variants of the TTB structure,[1] whose prototype is represented by $Ba_2NaNb_5O_{15}$, show a large nonlinear polarizability leading to useful electro-optical and nonlinear optical properties.[2,3]

By substituting oxygen with fluorine, the TTB structure becomes accessible to lower valence transition metals supporting unpaired *d* electrons, opening the way to magnetism. Fluorides with TTB structure, having general formula $K_xM^{II}_xM^{III}_{1-x}F_3$ with $0.4<x<0.6$, were first reported by De Pape[4] in 1965. Similar TTB phases have been reported to form for M=Fe or V,[4,5] and in the mixed systems Co/Fe, Mn/Fe, and Mn/Cr.[6–8] They have also been extensively studied because of the frustrated magnetic ordering[6,8–13] that arises at low temperature. The existence of ferroelectricity in TTB fluorides has been first reported for $K_{0.6}FeF_3$ and it has been related to its orthorhombic distortion of the TTB cell.[14,15] The possible coexistence of electric and magnetic orderings in TTB fluorides makes these materials potential magnetoelectric multiferroic systems.

In a recent work we investigated the structural properties of a series of iron and manganese based $K_xM^{II}_xM^{III}_{1-x}F_3$ TTB fluorides by transmission electron microscopy and electron diffraction.[16] The results, coupled with an accurate structure analysis performed by single-crystal x-ray diffraction (XRD) on $K_{0.53}FeF_3$, revealed unique structural features that are typical for all these materials. This leads to a unified structural description where charge order (CO) and cooperative tilt of the MF_6 octahedra modulations coexist; each one with its own periodicity differently commensurate to the conventional TTB cell. Charge ordering involves the perovskite unit of the TTB structure, which is built by MF_6 octahedra in such a manner that the larger divalent cations alternate with the smaller trivalent ones to reduce the structural stress. This gives rise to a superstructure named charge order superstructure (COS), which is twice in volume with respect to the fundamental TTB cell. On the contrary the tilt modulation extends on a larger periodicity, giving rise, in case of the examined crystal, to an orthorhombic supercell named ferroelastic superstructure (FES), which is eight times in volume than the fundamental TTB cell. This modulation is strictly similar to that found at room temperature (RT) in ferroelectric $Ba_2NaNb_5O_{15}$ (Ref. 17) where it is related to the appearance of ferroelasticity. Basing on the structural results of the single-crystal XRD analysis, which indicates $K_{0.53}FeF_3$ to be ferroelectric, such modulation can be considered generally distinctive of a ferroelectric-ferroelastic structure common to TTB niobates and transition-metal fluorides. As a consequence, coexistence of charge and ferroic [ferroelastic, ferroelectric, and ferrimagnetic (FM)] orders is expected in the low-temperature region over the whole compositional range of TTB fluorides, making these bronzes a model system to study complex ordering phenomena.

In this work we report the growth of K_xFeF_3 single crystals with the highest stoichiometry of potassium ($x>0.56$) for which a macroscopic orthorhombic distortion of the fundamental TTB cell has been reported at room temperature. This induced us to carry out a detailed structural investigation by a synergic use of different diffraction techniques, such as single-crystal and powder XRD, powder neutron diffraction, and electron diffraction. Measurements were performed by varying the temperature from RT to low temperatures (ranging from 4 to 100 K), well below the magnetic transition occurring around 120 K. The results allowed us to define the interesting phase diagrams of the system involving charge and ferroic orders, and confirmed its complete multiferroic nature below the magnetic transition.

II. EXPERIMENT

A series of fluorides with nominal compositions $K_xFe^{II}_xFe^{III}_{1-x}F_3$ ($0.56<x<0.60$) were prepared by solid-state reaction. Stoichiometric quantities of elementary fluorides (Aldrich Chemicals) were carefully mixed and grounded, mechanically sealed in Ag tubes, and fired under nitrogen atmosphere at 700 °C for a time of about 12 h. Reaction products were identified by powder XRD analysis. Crystals of composition quite close to $K_{0.6}FeF_3$ were obtained by partial melting of powder samples containing a 10% KF excess. The reagents grounded together in stoichiometric parts were heated up to 800 °C in N_2 atmosphere; crystal growth was then promoted by slow cooling (50 °C/h) in a thermal gradient. Single crystals exceeding 1 mm^3 were mechanically extracted from the solidified mass. Alternatively, single crystals were grown in hydrothermal conditions. The nutrient material (about 100 mg of $K_{0.6}FeF_3$ previously obtained via solid-state reaction), added to 10 μl of HF 40%, was sealed in a platinum tube (15 mm in length and 3 mm in diameter) and placed in a hydrothermal Leco Corp. apparatus with maximum reachable pressure $P_{max}=4$ Kbar. Temperature and pressure were slowly increased to 680 °C and 1.3 Kbar, respectively. The system was kept at these conditions for 96–144 h and finally cooled, releasing simultaneously the pressure. Dark red prismatic K_xFeF_3 crystals, elongated along the TTB *c* axis and ranging from few hundredth of micrometers to few millimeters in length, were grown in different experiments together with pale $KFeF_3$ perovskite crystals as minority phase. The segregation of perovskite lowers the final concentration of potassium in the TTB phase, giving rise in the different growth experiments to K_xFeF_3 crystal with *x* values comprised between 0.59 and 0.54 depending on the amount of segregated perovskite phase.

Powder XRD patterns were collected using Cu K_α radiation with a Thermo ARL X'tra powder diffractometer equipped with a Thermo Electron solid-state detector to eliminate the incoherent background produced by fluorescence of Fe. Data collection was performed by 0.01°–0.02° steps with counting time of 3–10 s. Temperature-dependent experiments were performed in vacuum on the same diffractometer by using an Anton Paar TTK450 chamber directly controlled by the diffractometer software. Single-crystal XRD data were collected with Mo K_α radiation on a Bruker AXS Smart diffractometer, equipped with a charge coupled device (CCD) area detector and an Oxford 600 series cryosystem. Magnetic characterization was carried out using a Quantum Design superconducting quantum interference device (SQUID) magnetometer. Neutron powder-diffraction data were collected on the DB2 line at the ILL research facility. Electron diffraction and high-resolution electron microscopy were carried out using a Philips TECNAI F20 transmission electron microscope operating at 200 kV. The specimens were prepared by grinding the powder in isopropylic alcohol and evaporating the suspension on a copper grid covered with a holey carbon film.

III. RESULTS AND DISCUSSION

A. Charge order superstructure and charge order in $K_{0.6}FeF_3$

XRD analyses of the crystals grown both by partial melting and hydrothermal conditions, performed at RT, pointed out the efficiency of slow cooling in strongly reducing the presence of ferroelastic domains connected to the exchange of *a* and *b* axes of the orthorhombic fundamental TTB so that "single domain" crystal were found to exceed 1 mm^3 in a few cases. Preliminary data collected on different crystals show, beside the fundamental reflections, the presence of the typical COS satellites, leading to the doubling of the *c* axis ($a_{COS}=a_{TTB}, b_{COS}=b_{TTB}, c_{COS}=2c_{TTB}$): differently from the previously investigated $K_{0.53}FeF_3$ crystals,[16] no FES satellite was detected at RT for all the examined samples.

Intensity data were collected at RT from a crystal showing the closest stoichiometry to the ideal limit ($K_{0.593}Fe^{2+}_{0.593}Fe^{3+}_{0.407}F_3$, determined by refining the structure occupancy factors of potassium ions). COS cell is orthorhombic *Pba*2 with $a=12.751(1)$, $b=12.660(1)$, and $c=7.975(1)$Å. The structure was solved with SIR2002 (Ref. 18) and refined with SHELX97 (Ref. 19) software making use of anisotropic thermal parameters for all atoms; the results of the refinement are reported in Table I. The analysis of the Fe-F bond distances for the six symmetry independent Fe atoms, reported in Table II, suggests a charge ordering scheme where Fe^{2+} and Fe^{3+} ions tend to alternate along the *c* axis in order to minimize the distortion. The analysis of charge distribution calculated with CHARDIS (Ref. 20) (last column in Table I) leads to an accurate definition of the charge ordering pattern whose graphical representation is given in Fig. 3.

These data differ from what was experimentally found in the case of $K_{0.53}FeF_3$ where Fe^{2+} and Fe^{3+} alternate around the perovskite cage, and along the *c* axis, whereas the extra-perovskite site is statistically occupied. In the present case in which the trivalent cation is present in a large excess, such ordering of the perovskite cage would engage completely the divalent cations, leaving the extra-perovskite columns to the smaller Fe^{3+}, a situation that maximizes the structural stress produced by stacking the different structural components along the *c* axis (Fig. 1). Therefore both perovskite and extra-perovskite sites are engaged in the charge ordering, assuming different characteristic on adjacent layers: at $z\approx0.25$, the extra-perovskite site Fe1 is occupied by Fe^{2+}, whereas Fe^{2+} and Fe^{3+} alternate around the perovskite cage in the Fe3 and Fe5 sites, respectively. At $z\approx0.75$ the extra-perovskite site Fe2 is occupied by Fe^{3+}, whereas around the perovskite cages Fe4 and Fe6 are occupied statistically and by Fe^{2+}, respectively. This arrangement represents the best compromise to minimize the structural stress in the structural stacking.

B. Ferroelastic superstructure

In spite of the lack of direct evidences of FES in single-crystal XRD at RT, electron-diffraction patterns performed on selected area at RT (Fig. 2) evidenced the presence of very weak FES satellites beside the stronger COS features.

TABLE I. Crystal data, refinement, and atomic parameters for $K_{0.593}FeF_3$. U(eq) is defined as one third of the trace of the orthogonalized U_{ij} tensor. Q(ij) is the ionic charge calculated by CHARDIS99 (Ref. 20). Site occupation factors (s.o.f.) are equal to one except where noted.

Space group	*Pba*2		Reflections collected	10564	
Unit cell dimensions	$a=12.7512(10)$Å		Data/restraints/parameters	2380 / 1 / 216	
	$b=12.6600(10)$Å		Goodness of fit on F^2	0.997	
	$c=7.9750(10)$Å		R indices $[I>2\sigma(I)]$	$R_1=0.0397$, $wR_2=0.1083$	
Volume	1287.4(2)Å^3		R indices (all data)	$R_1=0.0501$, $wR_2=0.1152$	
	x	*y*	*z*	U_{eq}(Å^2)	Q(ij)
Fe1	1/2	0	0.2510(3)	0.0139(2)	1.957
Fe2	1/2	0	0.7502(3)	0.0139(2)	2.868
Fe3	0.4247(1)	0.2844(1)	0.2508(3)	0.0139(2)	2.039
Fe4	0.4228(1)	0.2875(1)	0.7505(3)	0.0138(2)	2.575
Fe5	0.2120(1)	0.0753(1)	0.2513(3)	0.0135(2)	2.987
Fe6	0.2141(1)	0.0771(1)	0.7510(3)	0.0137(2)	2.024
K1[a]	1/2	1/2	−0.0010(6)	0.0219(8)	1.020
K2[b]	0	0	0.5035(6)	0.0200(8)	1.018
K3	0.6719(2)	0.1704(2)	0.9996(7)	0.0511(9)	0.974
K4	0.1714(2)	0.3309(2)	0.4974(7)	0.0550(10)	0.970
F1	1/2	0	0.5077(18)	0.0390(19)	
F2	1/2	0	−0.0091(16)	0.0377(20)	
F3	0.4207(3)	0.2946(4)	−0.0060(13)	0.0302(12)	
F4	0.4225(3)	0.2925(4)	0.5004(13)	0.0341(12)	
F5	0.2046(3)	0.0758(4)	0.0053(13)	0.0356(14)	
F6	0.2088(3)	0.0772(4)	0.4898(12)	0.0353(14)	
F7	0.2739(2)	0.2158(2)	0.2483(13)	0.0255(6)	
F8	0.2787(2)	0.2243(2)	0.7464(13)	0.0266(7)	
F9	0.3407(2)	−0.0014(2)	0.2528(15)	0.0371(8)	
F10	0.3481(2)	−0.0091(2)	0.7480(14)	0.0320(7)	
F11	0.5151(2)	0.1546(2)	0.2516(15)	0.0299(6)	
F12	0.5028(2)	0.1530(2)	0.7489(27)	0.0322(7)	
F13	0.3564(2)	0.4344(2)	0.2472(15)	0.0272(6)	
F14	0.1402(2)	−0.0679(2)	0.7479(16)	0.0290(7)	
F15	0.5711(2)	0.3650(2)	0.2494(15)	0.0292(6)	
F16	0.0659(2)	0.1438(2)	0.7504(15)	0.0316(7)	

[a]s.o.f. for K1: 0.966(6)
[b]s.o.f. for K2: 0.960(6)

Their intensity progressively increases by lowering the temperature and, at 220 K, the FES satellites represent the dominant modulation feature of the electron-diffraction pattern. This behavior may be indicative of a phase transition occurring close to RT, involving the ferroelastic properties of the system. The discrepancy between XRD and electron-

TABLE II. Bond distances involving iron and fluorine atoms (Å). Avg. indicates the average bond length.

Fe1-F11	1.967(2)	Fe2-F2	1.920(13)	Fe3-F4	1.994(10)	Fe4-F3	1.944(10)	Fe5-F6	1.903(10)	Fe6-F10	2.027(2)
Fe1-F11	1.967(2)	Fe2-F1	1.934(14)	Fe3-F11	2.007(2)	Fe4-F12	1.985(2)	Fe5-F9	1.907(2)	Fe6-F5	2.032(10)
Fe1-F9	2.031(2)	Fe2-F12	1.937(2)	Fe3-F3	2.053(10)	Fe4-F4	1.996(10)	Fe5-F7	1.946(2)	Fe6-F8	2.037(2)
Fe1-F9	2.031(2)	Fe2-F12	1.937(2)	Fe3-F13	2.089(2)	Fe4-F14	2.000(2)	Fe5-F15	1.949(2)	Fe6-F14	2.064(2)
Fe1-F1	2.047(14)	Fe2-F10	1.941(2)	Fe3-F7	2.110(2)	Fe4-F8	2.004(2)	Fe5-F5	1.964(10)	Fe6-F16	2.070(2)
Fe1-F2	2.074(13)	Fe2-F10	1.941(2)	Fe3-F15	2.128(2)	Fe4-F16	2.021(2)	Fe5-F13	1.986(2)	Fe6-F6	2.084(10)
Avg.	2.019(6)	Avg.	1.935(6)	Avg.	2.063(5)	Avg.	1.992(5)	Avg.	1.943(5)	Avg.	2.050(5)

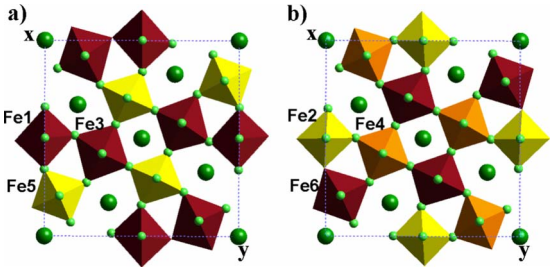

FIG. 1. (Color online) Charge ordering in the *ab* plane of the COS cell. The layers at $z \approx 1/4$ and 3/4 are shown in (a) and (b), respectively. Coordination octahedra surrounding Fe^{2+} and Fe^{3+} ions are evidenced in dark red (dark gray) and yellow (light gray), respectively; orange (medium gray) indicates the mixed-valence sites.

diffraction data could be related either to a small thermal difference in the corresponding experiments or to the smaller coherence length of the electron radiation, which is able to reveal structural periodicity on a shorter range (just at the onset of the phase transition).

Electron-diffraction patterns show a clear similitude between the FES modulation features of the examined samples, and those generally pointed out for $Ba_2NaNb_5O_{15}$ and the transition-metal TTB fluorides,[17] indicating a similar relation with the TTB cell. The main difference consists of a symmetry decrease from orthorhombic to monoclinic, related to the symmetry change of the fundamental TTB structure from tetragonal to orthorhombic, forcing the angle between the diagonals of the TTB *ab* plane (the axis directions in the FES structure) to differ from 90°. By taking into account the conventional monoclinic setting (unique axis *b*), the FES cell can be described by $a = 2\sqrt{(a_{\mathrm{TTB}}^2 + b_{TTB}^2)} \approx 35.94$, $b = 2c_{\mathrm{TTB}} \approx 7.96$, and $c = \sqrt{(a_{\mathrm{TTB}}^2 + b_{\mathrm{TTB}}^2)} \approx 17.97$ Å, where $\beta \approx 90.4°$. The appearance of a monoclinic FES near RT agrees with the results of Ishihara *et al.*[21] They performed optical and magnetic studies on ferroelectric $K_{0.6}FeF_3$ crystals grown by flux method. Polarized light microscopy pointed out the insurgence of phase transition at about 290 K characterized by a change in the ferroelastic domains from orthorhombic to monoclinic, in full agreement with the FES characteristics. The domains were found to persist below the magnetic transition (occurring at about 120 K), and the coupling of ferroelastic and magnetic orders was revealed by observation of anomalies in spontaneous linear birefringence at magnetic ordering temperature.

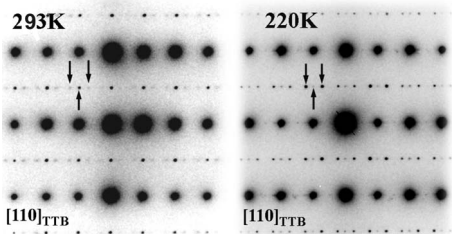

FIG. 2. Selected area electron-diffraction patterns collected in $[110]_{\mathrm{TTB}}$ zone axis at 293 (left) and 220 K (right). Downward and upward arrows indicate FES and COS modulation satellites, respectively.

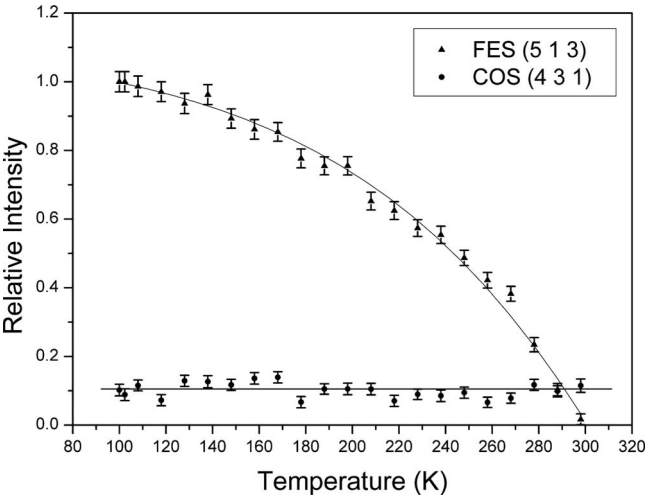

FIG. 3. Intensity variation of two typical modulation satellites (513 and 431, indexed on the basis of the FES and COS cells, respectively). Lines are a guide to the eye.

Knowing from electron diffraction the relationships between FES, COS, and TTB cells, a single-crystal XRD experiment was performed in the range of 300–100 K. The intensity of two selected satellite reflections, typical of FES and COS, respectively, were monitored by decreasing temperature and the results are shown in Fig. 3. FES satellites appear just below RT and, as revealed by electron diffraction, their intensity increases by decreasing temperature. No intensity saturation is observed in the examined temperature region, suggesting a progressive increase in the tilt modulation amplitude by decreasing *T*, even for temperatures below the magnetic transition. On the contrary the intensity of COS satellites remain constant, indicating the persistence of charge order on the whole temperature range. The occurrence of ferroelastic twinning domains, which are expected to exchange the a_{FES} and c_{FES} axes as reported in Fig. 4, was carefully investigated by measuring the intensity of the same satellite reflection for the two possible twinning variants. The results indicate an equiprobable occurrence of the twinning variants, which makes the refinement of the FES structure extremely difficult, limiting our approach to a qualitative description.

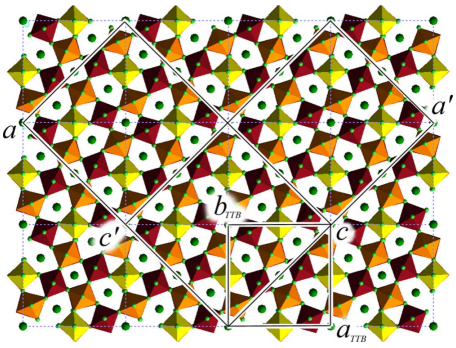

FIG. 4. (Color online) Relationships among the fundamental TTB lattice and the two possible twinning variants of FES.

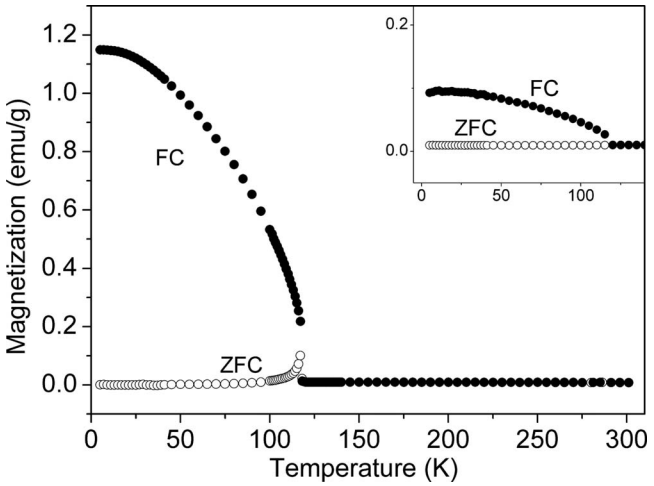

FIG. 5. Magnetization curves collected with applied field perpendicular and parallel (inset) to the c axis; FC and ZFC refer to field and zero-field cooling measurements.

C. Magnetic phase

SQUID measurement was performed on a $K_{0.6}FeF_3$ single crystal grown in hydrothermal conditions and the magnetization curves, measured by field and zero-field coolings with the magnetic field laying perpendicular and parallel to the c_{TTB} axis, are presented in Fig. 5. The behavior of the magnetization as a function of both the orientation on the magnetic field and of the cooling technique reveals a large anisotropy with the easy magnetization direction in the ab plane. $K_{0.6}FeF_3$ shows a ferrimagnetic behavior; the magnetic transition occurs at 118 K; the resultant magnetization, measured at $T=5$ K with an applied field $H=100$ Oe perpendicular and parallel to the c axis, is 1.15 and 0.09 emu/g, respectively. Neutron powder-diffraction patterns recorded at different temperatures ranging from 5 to 300 K are reported in Fig. 6. Magnetic peaks are observed below 118 K and can be indexed on the basis of the same COS cell used for the description of the charge ordering, in agreement with the results obtained on a Fe/Mn mixed compound.[10] However, if the 2θ region corresponding to the appearance of the magnetic peaks at lower temperature is considered, a significant increase in the background is observed well above the magnetic transition (starting from 200 K) and could be interpreted as being produced by short-range ordered magnetic interactions. These were reported to appear below 200 K in the isostructural system $KMnFeF_6$ (Ref. 22) where ^{19}F NMR studies suggest the presence of Dzyaloshinskii-Morya interaction, leading to out-of-ab-plane spin canting.

D. Multiferroic phase diagram

The dependence on the temperature of the fundamental TTB cell lattice parameters, as determined by neutron and x-ray powder-diffraction data, is reported in Fig. 7. A series of anomalies, consisting of discontinuities or, more simply, of a change in the expansion coefficient, are observed in the figure and can be related to phase transitions. The first two anomalies, observed by increasing the temperature around

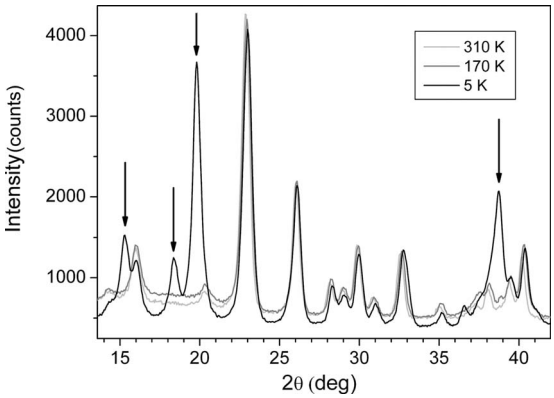

FIG. 6. Neutron powder-diffraction patterns taken at different temperatures. The main magnetic contributions are indicated by arrows.

118 and 290 K, are connected with the magnetic transition and the appearance of FES modulation, respectively, as previously discussed. The structural transition is located around 570 K whereas the assignment of the anomaly observed at 490 K is more complex. For a long time it has been believed that the latter temperature would be associated to a dramatic change in the structural properties of $K_{0.6}FeF_3$, leading simultaneously to the vanishing of charge order, ferroelectricity, and ferroelasticity. The loss of charge order, suggested by an inflection in resistivity at this temperature,[14] was then confirmed by Mössbauer measurements[23] showing a sharp change in slope of the temperature dependence of the Fe^{3+} quadrupolar splitting and isomer shift. The simultaneous occurrence of the ferroelectric-paraelectric transition at 490 K, associated to a change in symmetry from $mm2$ to $4/mmm$

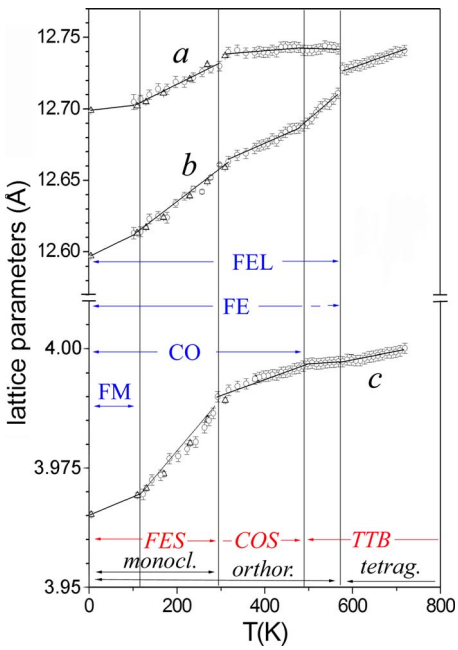

FIG. 7. (Color online) Thermal evolution of the fundamental TTB cell parameters of $K_{0.6}FeF_3$ in the range of 5–700 K; structural modifications and existence regions of ordering phenomena (FM, FE, FEL, and CO) are reported.

point group, and the disappearance of ferroelasticity was reported by Ravez *et al.*[14] on the basis of a maximum in the relative dielectric permittivity observed at this temperature. However, our XRD data unambiguously reveal that the orthorhombic-tetragonal structural transition is located 80 K above this temperature. Since the onset of ferroelasticity is associated to the appearance of the orthorhombic distortion, we conclude that the ferroelastic transition occurs at 570 K. For what concerns the permittivity maximum at 490 K and its assignment to the ferroelectric-paraelectric transition, it is interesting to note that a temperature dispersion of 10 K was observed in the original measurements[14] for the explored frequency range (0.1–10 KHz). Such dispersion, suggestive of dielectric relaxation, was interpreted as the signature of a relaxor ferroelectric. However, the simultaneous increase in the dielectric loss at higher temperature, resulting from the semiconducting character of the sample (further enhanced by the order-disorder transition), produces critical experimental conditions that could make the detection of further anomalies very difficult at higher temperatures.

IV. CONCLUSIONS

A detailed investigation of the structural properties of the TTB fluoride $K_{0.6}FeF_3$ was performed by a synergic use of different diffraction techniques, ranging from single-crystal and powder XRD to powder neutron diffraction and electron diffraction. Measures were performed by varying the temperature from RT to low temperatures (4–100 K), well below the magnetic transition occurring at 118 K. The results allowed us to define the interesting phase diagrams of the system involving charge and ferroic orders, and confirmed its complete multiferroic nature below the magnetic transition temperature. Below T_N the system, characterized by an ordered arrangement of the Fe^{2+} and Fe^{3+} cations, is simultaneously ferrimagnetic, ferroelectric, and ferroelastic. Above this temperature and until 200 K, the magnetic background observed in neutron-diffraction patterns suggests the presence of short-range ordered magnetic interactions whose nature is under investigation. The FES modulation, characteristic of ferroelasticity in the tetragonal members of the $K_xFe_x^{II}Fe_{1-x}^{III}F_3$ family, disappears at about 290 K. However, owing to the orthorhombic distortion of its TTB structure, $K_{0.6}FeF_3$ remains ferroelastic until 570 K where the orthorhombic-tetragonal transition takes place. Charge order involving Fe^{2+} and Fe^{3+} cations disappear at 490 K whereas the temperature of the ferroelectric-paraelectric transition is probably located between 490 and 570 K, depending on its association to the order-disorder or to the orthorhombic-tetragonal phase transition. Further work is necessary to clarify this point but permittivity measurements in this temperature region are made difficult by the increase in electrical conductivity.

ACKNOWLEDGMENTS

We thank the Institute Laue-Langevin (Grenoble, France) for providing technical and financial support. In particular the authors are grateful to M. T. Fernández-Díaz for the experimental support during neutron-diffraction experiments.

*Corresponding author. calestg@unipr.it

[1] P. B. Jamieson, S. C. Abrahms, and J. L. Bernstein, J. Chem. Phys. **48**, 5048 (1968).
[2] J. E. Geusic, H. J. Levinstein, S. Singh, R. G. Smith, and L. G. Van Uitert, Appl. Phys. Lett. **12**, 306 (1968).
[3] R. G. Smith, J. E. Guesic, H. J. Levinstein, J. J. Rubin, S. Singh, and L. G. Van Uitert, Appl. Phys. Lett. **12**, 308 (1968).
[4] R. De Pape, C. R. Hebd. Seances Acad. Sci. **260**, 4527 (1965).
[5] R. F. Williamson and W. O. Boo, Inorg. Chem. **16**, 649 (1977).
[6] S. Giri and K. Ghoshray, Phys. Rev. B **57**, 5918 (1998).
[7] E. Banks, S. Nakajima, and G. J. B. Williams, Acta Crystallogr., Sect. B: Struct. Crystallogr. Cryst. Chem. **35**, 46 (1979).
[8] E. Banks, M. Shone, Y. S. Hong, R. F. Williamson, and W. O. J. Boo, Inorg. Chem. **21**, 3894 (1982).
[9] E. Banks, M. Shone, R. F. Williamson, and W. O. J. Boo, Inorg. Chem. **22**, 3339 (1983).
[10] P. Lacorre, J. Pannetier, and G. Ferey, J. Magn. Magn. Mater. **94**, 331 (1991).
[11] S. Giri, K. Ghoshray, A. Ghoshray, and N. Chatterjee, J. Magn. Magn. Mater. **157-158**, 411 (1996).
[12] S. Mohammad Yusuf, L. Madhav Rao, R. Mukhopadhyay, S. Giri, and K. Ghoshray, Solid State Commun. **101**, 145 (1997).
[13] S. C. Bhargava, S. Singh, A. H. Morrish, and Z. W. Li, Solid State Commun. **116**, 575 (2000).
[14] J. Ravez, S. C. Abrahams, and R. De Pape, J. Appl. Phys. **65**, 3987 (1989).
[15] J. Ravez, S. C. Abrahams, A. M. Mercier, L. Rabardel, and R. De Pape, J. Appl. Phys. **67**, 2681 (1990).
[16] S. Fabbrici, E. Montanari, L. Righi, G. Calestani, and A. Migliori, Chem. Mater. **16**, 3007 (2004).
[17] P. Labbè, H. Leligny, B. Raveau, J. Scheck, and J. C. Toledano, J. Phys.: Condens. Matter **2**, 25 (1990).
[18] A. Altomare, M. C. Burla, M. Camalli, G. Cascarano, C. Giacovazzo, A. Guagliardi, A. G. G. Moliterni, G. Polidori, and R. Spagna, *SIR2002, Program for Crystal Structure Solution and Refinement* (IRMEC-CNR, Bari, Italy, 2002).
[19] G. M. Sheldrick, *SHELXL93, Program for the Crystal Structure Refinement* (University of Gottingen, Germany, 1993).
[20] M. Nespolo, G. Ferraris, and H. Ohashi, Acta Crystallogr., Sect. B: Struct. Sci. **55**, 902 (1999).
[21] S. Ishihara, J.-P. Rivera, E. Kita, Z.-G. Ye, F. Kubel, and H. Schmid, Ferroelectrics **162**, 51 (1994).
[22] S. Giri, K. Ghoshray, A. Ghoshray, and N. Chatterjee, Phys. Rev. B **56**, 3347 (1997).
[23] Y. Calage, S. C. Abrahams, and J. Ravez, J. Appl. Phys. **67**, 430 (1990).